Title
Electron-Withdrawing Effects in the Photodissociation of CH2ICl To Form CH2Cl Radical, Simultaneously Viewed Through the Carbon K and Chlorine L2,3 X-ray Edges

Journal
Journal of the American Chemical Society, 140(41)

ISSN
0002-7863

Authors
Yang, Zheyue
Schnorr, Kirsten
Bhattacherjee, Aditi
et al.

Publication Date
2018-10-17

DOI
10.1021/jacs.8b08303

Peer reviewed

JACS
JOURNAL OF THE AMERICAN CHEMICAL SOCIETY
Article
Cite This: J. Am. Chem. Soc. 2018, 140, 13360−13366
pubs.acs.org/JACS

Electron-Withdrawing Effects in the Photodissociation of CH_2ICl To Form CH_2Cl Radical, Simultaneously Viewed Through the Carbon K and Chlorine $L_{2,3}$ X-ray Edges

Zheyue Yang,[†,‡] Kirsten Schnorr,[†,‡,#] Aditi Bhattacherjee,[†,‡,⊥] Pierre-Louis Lefebvre,[§] Michael Epshtein,[†,‡] Tian Xue,[†,‡] John F. Stanton,[§] and Stephen R. Leone*[,†,‡,∥]

[†]Department of Chemistry, University of California, Berkeley, California 94720, United States
[‡]Chemical Sciences Division, Lawrence Berkeley National Laboratory, Berkeley, California 94720, United States
[§]Quantum Theory Project, Departments of Chemistry and Physics, University of Florida, Gainesville, Florida 32611, United States
[∥]Department of Physics, University of California, Berkeley, California 94720, United States

Supporting Information

ABSTRACT: A fundamental chlorine-containing radical, CH_2Cl, is generated by the ultrafast photodissociation of CH_2ICl at 266 nm and studied at both the carbon K edge (~284 eV) and chlorine $L_{2,3}$ edge (~200 eV) by femtosecond X-ray transient absorption spectroscopy. The electronic structure of CH_2Cl radical is characterized by a prominent new carbon 1s X-ray absorption feature at lower energy, resulting from a transition to the half-filled frontier carbon 2p orbital (singly occupied molecular orbital of the radical; SOMO). Shifts of other core-to-valence absorption features upon photodissociation of CH_2ICl to yield $\cdot CH_2Cl$ indicate changes in the energies of core-level transitions of carbon and chlorine to the σ^*(C−Cl) valence orbital. When the C−I bond breaks, loss of the electron-withdrawing iodine atom donates electron density back to carbon and shields the carbon 1s core level, resulting in a ~0.8 eV red shift of the carbon 1s to σ^*(C−Cl) transition. Meanwhile, the 2p inner shell of the chlorine atom in the radical is less impacted by the iodine atom removal, as demonstrated by the observation of a ~0.6 eV blue shift of the transitions at the chlorine $L_{2,3}$ edges, mainly due to the stronger C−Cl bond and the increased energy of the σ^*(C−Cl) orbital. The results suggest that the shift in the carbon 1s orbital is greater than the shift in the σ^*(C−Cl) orbital upon going from the closed-shell molecule to the radical. Ab initio calculations using the equation of motion coupled-cluster theory establish rigorous assignment and positions of the X-ray spectral features in the parent molecule and the location of the SOMO in the CH_2Cl radical.

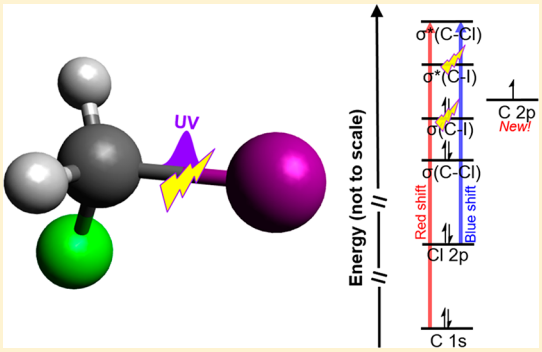

INTRODUCTION

Radicals, characterized by partially filled orbitals, have triggered much interest due to their transient nature and ubiquitous role in chemical reactivity. Halogenated radicals, in particular, are common intermediates and byproducts in combustion and atmospheric processes and constitute an important subgroup that has been given significant attention over the last decades.[1−3] As one of the most representative radicals of this kind, CH_2Cl radical has been proposed, with various mechanisms, to be an inhibitor in the combustion of chlorinated fuels,[1] an origin of soot formation,[4] as well as a key to possible disposal pathways of NO_2,[5] a deleterious byproduct of combustion. Halogenated radicals have also been in the spotlight due to their role in environmental processes. They are involved in stratospheric processes such as ozone depletion,[6] in addition to marine decomposition where boundary aqueous layers react with these radicals to a non-negligible extent.[4] It is fundamental to explore the electronic structures and energetics of these transient species, which are usually difficult to capture in reactions.

Ultrafast laser techniques, especially transient absorption spectroscopy, provide a robust way to study short-lived reaction intermediates. Selective bond-breaking, made possible by photodissociation at a specific wavelength, produces desirable transient species in a consistent fashion. In particular, the C−I bond, known to dissociate at approximately 270 nm, can be utilized to form specific radicals from iodine-containing organic molecules.[7] Furthermore, transient absorption spectroscopy, as opposed to electron or ion spectroscopy, is capable of detecting not only charged species but also neutral ones, thus allowing studies of the altered electronic structure resulting from neutral dissociation or ionization. Recent progress toward core-level spectroscopy centered on the

Received: August 3, 2018
Published: September 24, 2018

DOI: 10.1021/jacs.8b08303
J. Am. Chem. Soc. 2018, 140, 13360−13366

carbon K edge demonstrates the power of using X-ray spectroscopic techniques to study the dynamics and the electronic structures of transient species.[8−10]

The UV spectrum of CH_2ICl, like other C−I containing molecules, has a characteristic A band absorption corresponding to the electronic transition from the localized nonbonding iodine atomic orbitals n(I) to the σ^*(C−I) molecular orbital.[7,11−13] The potential energy surface of CH_2ICl resembles that of CH_3I where the 3A′ state (equivalent to the $^3Q_0$ state in CH_3I but with a lower symmetry) is excited at ∼270 nm and leads to a major channel dissociating into $\cdot CH_2Cl$ and $I^*(^2P_{1/2})$ and a minor one into $\cdot CH_2Cl$ and $I(^2P_{3/2})$ by passage through a conical intersection, both of which take place within 150 fs.[12] In the pump−probe experiment here, a 266 nm-pump pulse is used to first initiate the C−I bond cleavage of CH_2ICl and broad band soft X-ray pulses then probe the electronic structure of the product $\cdot CH_2Cl$ by transient absorption spectroscopy. The transient radical species is thus characterized from the perspectives of both the carbon and the chlorine atoms by spectroscopic investigations on their core−shell transitions (1s and 2p, respectively).

As the iodine atom departs the parent CH_2ICl molecule and a CH_2Cl radical is formed, the primary effect on the carbon atom as well as a secondary effect on the chlorine atom are captured simultaneously through shifts in the core-to-valence transitions. Iodine, as a strongly electron-withdrawing element, significantly impacts the oxidation state of the carbon atom by bonding, which is reflected in a shift of the carbon core level. The molecular geometry will also accommodate the departure of iodine, allowing more space for carbon-chlorine bonding, strengthening the C−Cl bond, and consequently changing the valence orbital energy levels. Chlorine, while not directly affected by the electronegativity of iodine, experiences this change through the valence bonding and antibonding orbitals. Since both the carbon and chlorine core level transitions couple to the same σ^*(C−Cl) antibonding orbital, these energy shifts upon going from the closed-shell molecule to the radical are obtained directly in the experiment and corroborated by electronic structure calculations.

EXPERIMENTAL METHODS

The apparatus to generate the pump pulse of 266 nm and broadband X-ray probe pulse has been described elsewhere.[8,9] In brief, the output of a 12 mJ per pulse, 800 nm-centered, 1 kHz repetition rate, 35 fs Ti:Sapphire femtosecond laser is split into two branches in a 9:1 ratio. The 10% branch is used to produce third harmonic generation with two nonlinear crystals to generate ultraviolet pulses centered at around 266 nm. The other 90% is used as a pump for a tunable traveling-wave optical parametric amplifier of superfluorescence (TOPAS), which is tuned to output infrared light at 1320 nm with a pulse energy of 2.5−2.8 mJ. These near-infrared pulses are subsequently focused by a 40 cm lens into a semi-infinite gas cell filled with 750−800 Torr of helium to emit soft X-ray light ranging from 150 to 300 eV through the high harmonic generation (HHG) process. The residual infrared light is blocked by a 100 nm-thick aluminum filter, whereas the soft X-ray radiation is transmitted and further focused by a toroidal mirror. The 266 nm ultraviolet (UV) pump beam is attenuated by a neutral density filter and focused by a 45 cm lens where the pulse energy can be adjusted between 10 and 30 μJ and the pump intensity between 2 and 5×10^{11} W/cm^2. The soft X-ray and the UV beam overlap at an angle of approximately 1° within a flowing gas cell containing the CH_2ICl sample purchased from Sigma-Aldrich and used at ∼ 60 °C (vapor pressure ∼150 Torr, entire gas line heated) after freeze−pump−thaw degassing. The soft X-ray beam is transmitted by the gas cell, diffracted by an X-ray grating onto a charged-couple device (CCD) camera chip with 1340 × 400 pixels (Figure S1), and the UV beam is blocked by a 100 nm-thick titanium filter after the gas cell to prevent pump scattering.

A static absorption spectrum of a target gas is recorded with 1 s of camera exposure time and with the soft X-ray beam only, using the spectrum without the target gas as a background. The resultant spectrum of the parent molecule CH_2ICl, averaged over 64 such sets (64,000 pulses in total with gas, 64,000 without) for improved statistics, is then calculated according to the Beer−Lambert law where

$$\text{absorbance}_{\text{target gas}} = -\log_{10}\frac{\text{flux}_{\text{x-ray}}(\text{with gas})}{\text{flux}_{\text{x-ray}}(\text{without gas})}$$

A transient absorption spectrum is recorded with 1 s of camera exposure time with both the pump UV and the probe soft X-ray beam, the delay time between which is controlled by a motorized stage to include 50 time points in between −300 fs (X-ray preceding UV) and 1000 fs (UV preceding X-ray), using the absorption spectrum without the pump UV beam as a background. The change between the two yields a transient spectrum where

$$\Delta\text{absorbance}_{\text{target gas,delay timepoint}} = -\log_{10}\frac{\text{flux}_{\text{x-ray}}(\text{with gas, with UV})}{\text{flux}_{\text{x-ray}}(\text{with gas, without UV})}$$

and averaged over at least 32 such sets (32,000 pulses with UV, 32,000 pulses without UV at each time delay point) for statistics, which takes typically two hours for 50 points overall.

The energy scale for all spectra is calibrated using known core-to-valence transitions in argon,[14] carbon disulfide,[15,16] and methyl iodide.[17] The spectral resolution is determined to be 360 ± 20 meV by the Gaussian broadening of the $2p_{3/2} \rightarrow 4s$ transition in argon to match the observed spectra, assuming the core−hole lifetime broadening is 120 meV (Figure S2).[14] The temporal resolution is estimated to be 90 ± 10 fs based on the ponderomotive shift of the $2p_{3/2} \rightarrow 4s$ transition in argon (Figure S3).[9]

The core-level excited states of CH_2ICl and CH_2Cl are calculated with the techniques of coupled-cluster theory. For CH_2ICl, which has a closed-shell ground state, excitation energies are obtained with the equation of motion coupled-cluster theory (EOM-CCSD)* method,[18,19] in conjunction with the SFX2C-1e treatment of relativistic effects[20−22] (which are important in the treatment of core-level processes, even in the carbon atom) with relativistic atomic natural orbital basis sets (ANORCC)[23] of triple-ζ quality, truncated to 5s4p2d1f on Cl, 7s6p4d2f1g on I, 4s3p2d1f on C, and 3s2p1d on H.[24] Oscillator strengths are also obtained with the same basis sets and SFX2C-1e, but only at the CCSD level. For the CH_2Cl radical, the X-ray excitation energy is computed by taking the difference between the ground-state energy and the excited-state energy, the latter being calculated using EOMIP-CCSDT theory[25] using the CH_2Cl anion as the reference state. The SFX2C-1e treatment of relativistic effects and the basis sets listed above were again used. All calculations are performed with the CFOUR program suite[24] in the frozen-core approximation, in which all electrons lower in energy than the carbon 1s and chlorine 2s orbitals are omitted from the correlation part of the calculation. In addition, all calculations are performed at geometries optimized at the MP2 level with the SFX2C-1e treatment, and the basis sets listed above.

RESULTS AND DISCUSSION

Static Soft X-ray Absorption Spectra of CH_2ICl. Figure 1a,b shows representative static absorption spectra of CH_2ICl at the carbon K (1s) edge and the chlorine $L_{2,3}$ (spin−orbit split $2p_{1/2}$ and $2p_{3/2}$) edges, respectively, acquired as described earlier. To our knowledge, no Cl L edge or C K edge absorption spectra of CH_2ICl have been reported, and assignments are based on peaks observed in similar halogenated molecules (CH_3Cl and CH_3I) and complementary computations shown in Tables 1 and 2.

DOI: 10.1021/jacs.8b08303
J. Am. Chem. Soc. 2018, 140, 13360−13366

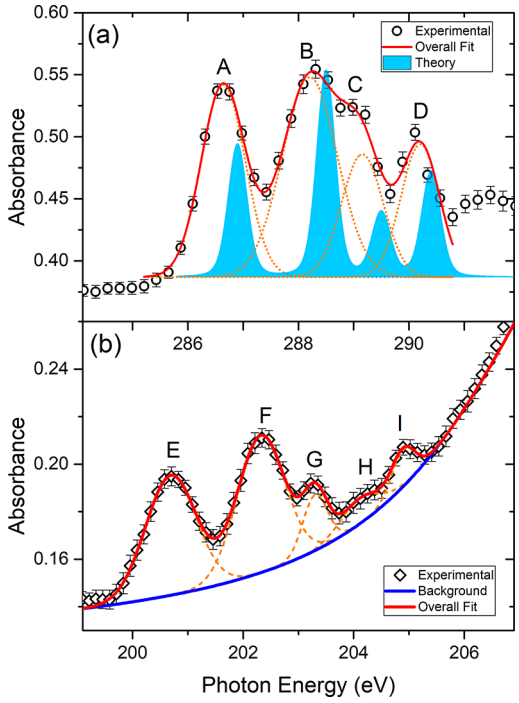

Figure 1. Static absorption spectra of CH_2ICl at (a) carbon K edge and (b) chlorine $L_{2,3}$ edges where the orange dash lines are Gaussian fits to the peaks, the red solid lines summation of all the fitted peaks, the shaded blue area is computational results convoluted with instrumental spectral resolution and the core−hole lifetime from Alagia et al.[26] and scaled with respect to the experimental absorbance, and the blue solid line the extrapolated background (due to core photoionization). The actual core−hole lifetime may be different. Additionally, the experimental peaks can be broadened due to vibronic coupling. The spectral resolution reported here is not able to resolve these fine details, and the theoretical ones only compute the transitions from the electronic ground state to the ground core−hole state. Peaks A−F are assigned as in Table 1. An overview across the whole spectral range is shown in Figure S4.

Table 1. Assignments of Spectral Features Observed at C K Edge and Cl $L_{2,3}$ Edges of CH_2ICl[a]

peak	exptl. energy (eV)	exptl. ref. energy (eV) (ref. molecule)	assignment
A	286.6 ± 0.1	285.6 (CH_3I)[17]	C(1s) → σ*(C−I)
B	288.2 ± 0.1	287.3 (CH_3Cl)[17]	C(1s) → σ*(C−Cl)
C	289.1 ± 0.1	–	C(1s) → σ*(C−H)
D	290.0 ± 0.1	–	C(1s) → σ*(C−H)
E	200.6 ± 0.1	200.8 (CH_3Cl), 200.8 (CH_2Cl_2), 200.6 ($CHCl_3$), 200.5 (CCl_4)[27−29]	Cl($2p_{3/2}$) → σ*(C−Cl)
F	202.3 ± 0.1	202.4 (CH_3Cl), 202.9 (CH_2Cl_2), 202.4 ($CHCl_3$), 202.4(CCl_4)[27,29]	Cl($2p_{1/2}$) → σ*(C−Cl)

[a]Peak positions are reported as the averaged Gaussian fitting results of spectra reproduced on different days. The errors are one standard deviation from these spectra convoluted with Gaussian fitting errors.

In the carbon K edge region, peaks A and B are separated by 1.6 eV, which is the same difference between the reported values for the C(1s) → σ*(C−I) transition in CH_3I and the C(1s) → σ*(C−Cl) transition in CH_3Cl from electron scattering studies.[17] However, peaks A and B are ∼1 eV blue-shifted from the C(1s) → σ*(C−I) in CH_3I and the C(1s) → σ*(C−Cl) in CH_3Cl, respectively. This leads to the assignment of peak A to the C(1s) → σ*(C−I) and peak B to the C(1s) → σ*(C−Cl) in CH_2ICl. The 1 eV shifts from the monohalomethanes are understood as the additional electron-withdrawing effect from the central carbon atom because there are two halogen atoms instead of one, making the carbon atom more electron deficient and leading to a stronger Coulomb attraction between the nucleus and the carbon 1s electrons. The energy thus required to excite an electron from the carbon core level to valence antibonding orbitals is increased by 1 eV. Additionally, based on the EOM-CCSD from which predictions of peak positions and oscillator strengths convoluted with spectral resolution as well as orbital pictures are shown in Table 2, peak A displays a C−I antibonding nature, whereas peak B signifies C−Cl antibonding and peaks C and D C−H antibonding. Peak separations match extremely well with the experimental data, although the absolute energies from the computations are in general 0.3−0.4 eV higher. Similar relative shifts with respect to the respective monohalogenated methanes suggest that the antibonding character is preserved in CH_2ICl.

In comparison, peaks E and F observed at the chlorine L_3 ($2p_{3/2}$) and L_2 ($2p_{1/2}$) edges, respectively, are very close to the values of the excitation energies of Cl 2p → σ*(C−Cl) transitions observed in CH_3Cl, CH_2Cl_2, $CHCl_3$, and CCl_4,[27−29] as listed in Table 1. This highlights the well-known sensitivity of the X-ray absorption spectrum to the localized oxidation state of the reporter atom, as the oxidation state of carbon is significantly more greatly changed upon additional halogenation than the neighboring halogen atoms. The 1.7 eV difference between E and F is consistent with the Cl 2p inner shell spin−orbit splitting observed in these species. The population ratio of the two spin−orbit components is not following the degeneracy factor (2:1) possibly due to multiplet effects which in particular occurs at soft X-ray edges where these core orbitals can overlap with valence orbitals, as reported by de Groot.[30] Peaks G and I constitute another spin−orbit pair, which may correspond to transitions to higher lying Rydberg states (such as 4s), according to previous literatures.[27−29] A weak and broad feature, observed as peak H, remains unassigned at present.

To summarize, by promoting an electron from one of the core orbitals to one vacant valence orbital, core-level spectroscopy not only offers information about the energy difference between core shell and valence shell but also the relative difference among the valence orbitals.

Transient Absorption Spectra of CH_2ICl: Formation of CH_2Cl Radical As a Photodissociation Product. Representative transient absorption spectra of CH_2ICl obtained as mentioned earlier and integrated at long delay time points between 400 and 1000 fs are shown in Figure 2. CH_2ICl is known to have a C−I bond dissociation time scale of 100−150 fs,[12,13] as verified by the temporal dependence of the features shown in Figure S5. Hence at 400 fs, long after the photodissociation is complete, the spectra reflect absorption of the photodissociation products and depletion of the parent molecule. Positive-going features represent new species that occur when UV light excites and dissociates CH_2ICl, and negative features indicate changes in the static spectrum when the CH_2ICl molecules are depleted by UV excitation.

A new strong positive feature in the carbon K edge region at 282.8 ± 0.1 eV, peak J, is observed and accompanied by two broad shoulder features M and N at ∼284 eV. CH_2ICl

DOI: 10.1021/jacs.8b08303
J. Am. Chem. Soc. 2018, 140, 13360−13366

Table 2. Absorption of CH_2ICl at Carbon K Edge Based on EOM-CCSD* Calculations

Peak	A	B	C	D
Energy	286.9 eV	288.5 eV	289.5 eV	290.4 eV
Oscillator Strength	0.029	0.045	0.014	0.023
Orbital	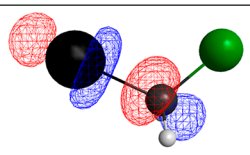	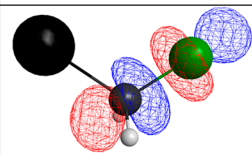	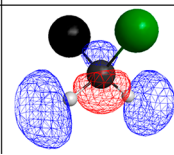	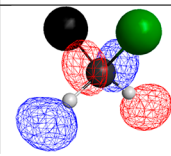

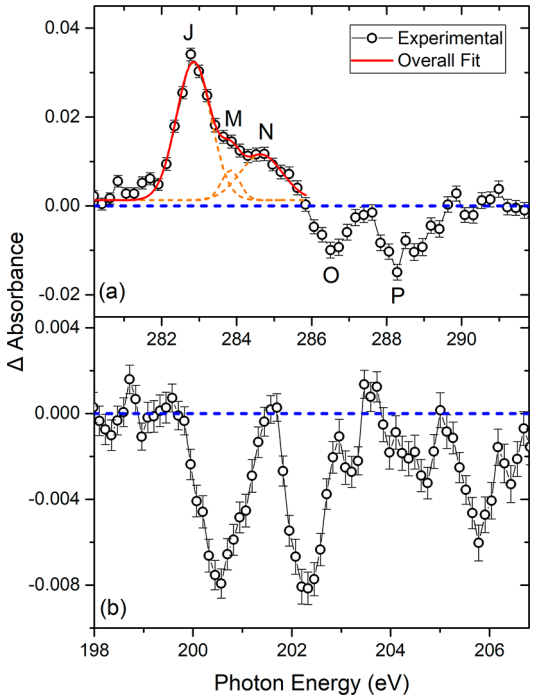

Figure 2. Transient absorption spectra of CH_2ICl at (a) carbon K edge where the orange lines are deconvoluted Gaussian peaks and the red line summation of all the fitted peaks and (b) chlorine $L_{2,3}$ edges. The blue lines are reference zero lines.

photodissociation at 266 nm is dominated by direct dissociation when an iodine 5p electron is promoted to the σ^*(C−I) orbital, leading to electronically repulsive states and photodissociation products of CH_2Cl and I or I*.[12] Along the photodissociation coordinate, the σ^*(C−I) orbital is broken into nonbonding I 5p and C 2p orbitals. Peak J is thus attributed to the transition of C(1s) → C(2p) in the CH_2Cl radical, as the C 2p orbital of the radical is singly occupied. According to the calculations outlined earlier, this core to the singly occupied molecular orbital (SOMO) transition occurs at 282.8 eV and strongly resembles a carbon 2p orbital, perfectly matching the experimental observations. It is worth noting that this transition is 1.5 eV higher in energy than the C(1s) → C(2p) transition observed in CH_3,[26] and this difference of 1.5 eV can be rationalized by the electron-withdrawing effect of chlorine on the carbon atom. The result is also consistent with the 1.5 eV difference found in the carbon 1s ionization potentials between CH_4 (290.8 eV) and CH_3Cl (292.3 eV) reported in the literature.[12]

Features M and N are determined to be related to nonlinear (multiphoton) absorption processes. The dependence of both peaks on the UV power, in comparison with peak J, is demonstrated in Figure 3, where the log of peak intensity is

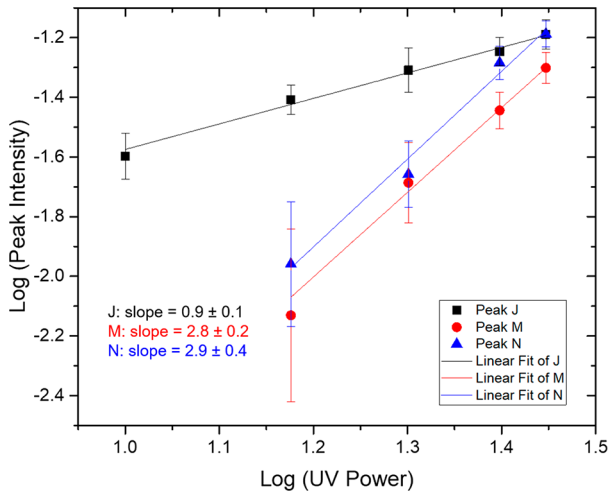

Figure 3. Power dependence studies of peaks J, M, and N with respective log−log linear fits.

plotted versus the UV excitation power. Peak J results in a slope of 0.9 ± 0.1, whereas M and N have a slope of 2.8 ± 0.2 and 2.9 ± 0.4, respectively, a sign of multiphoton processes.[31] One possible source of M and N is ionization of CH_2ICl, which requires three photons.[32] Upon ionization, one electron will be ejected from one of the valence bonding orbitals, and these fully occupied orbitals will become half-filled. Peaks M and N could represent absorptions to these half-filled bonding orbitals, and thus they are at lower energies than peaks A and B in the static absorption spectrum (Figure 1), which results from absorptions to antibonding orbitals. Dissociative ionization could also be a possibility,[33] but at this time we are not able to make a definitive assignment of peaks M and N.

Turning to the negative-going features, peak O matches the position of peak A in Figure 1. As the C−I bond is broken when CH_2ICl photodissociates at 266 nm, this depletion corresponds to the removal of the C(1s) → σ^*(C−I) absorption of the parent molecule after the photodissociation process is complete. More intriguingly, negative features, peaks P at carbon and Q and R at chlorine also show up around the positions of C(1s) → σ^*(C−Cl) and Cl(2p) → σ^*(C−Cl), respectively (i.e., peaks B, F, and G, respectively). The n(Cl) → σ^*(C−Cl) transition leading to C−Cl bond cleavage occurs at ∼170 nm, which should only contribute to a very minor portion of this depletion.[11] Changes in the C(1s), Cl (2p) → σ^*(C−Cl) transition energies, however, are highly likely, given that the reactant, CH_2ICl, and the product, CH_2Cl, exhibit

DOI: 10.1021/jacs.8b08303
J. Am. Chem. Soc. 2018, 140, 13360−13366

changing electronic configurations of the carbon atom, which would perturb the energy levels of carbon 1s and chlorine 2p as well as σ^*(C−Cl), as a result.

In order to determine the exact shifts of the C(1s), Cl($2p_{3/2}$), Cl($2p_{1/2}$) → σ^*(C−Cl) transitions, proportions of a static parent molecule spectrum are added back to the transient absorption spectrum (where only a moderate UV power is used so that the ion features M and N are suppressed as demonstrated in Figure S6) to obtain a pure spectrum of the photodissociation products; the added back spectral result is shown in Figure 4. The proportions are controlled so that the

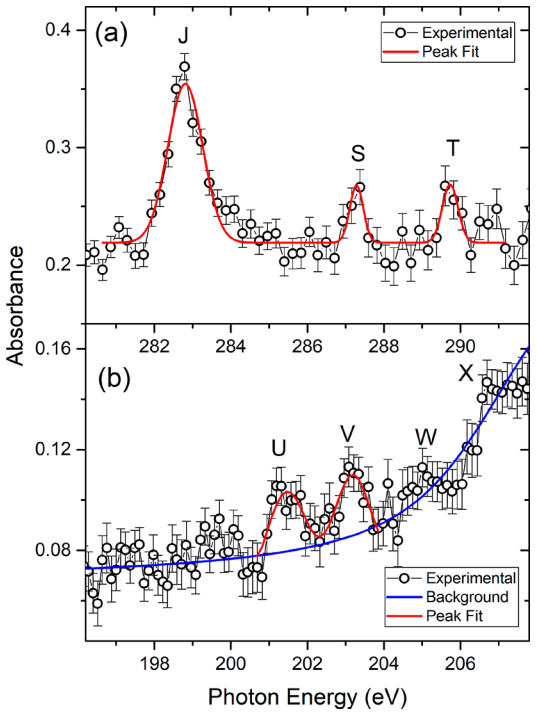

Figure 4. Summation of Figures 1 and 3 spectra, respectively, with controlled proportion so that the signal corresponding to the C(1s) → σ^*(C−I) transition in CH_2ICl is removed to the baseline level, which reveals the pure absorption spectrum of the photodissociation product, CH_2Cl, taken at low UV pump intensity so that the ion spectral features are minimized, at (a) carbon K edge and (b) chlorine $L_{2,3}$ edges, where the blue line is the extrapolated background and the red lines are peak fits. Peaks J and S−V are assigned in Table 3.

area around peak A approaches a baseline level, as no transition of C(1s) → σ^*(C−I) from the parent molecule should be observed in the product.

In the added back spectrum, peaks S and T become visible at the carbon K edge. Peak S is assigned as C(1s) → σ^*(C−Cl) of the CH_2Cl radical; as removing the iodine atom from CH_2ICl will make the carbon nucleus less positively charged, hence more repulsive to the core electrons, the energy needed to promote electrons from the core level is decreased. Compared to peak B, peak S is red-shifted by 0.8 eV, similar to the energy difference in the C(1s) → σ^*(C−Cl) transition between CH_3Cl and CH_2ICl, as demonstrated earlier in Table 1. Peak T is likely a blue-shifted version of peak C or a red-shifted version of D, depending on the exact mixing nature of the Rydberg orbitals, which needs to be verified by further theoretical calculations.

Turning to the chlorine $L_{3,2}$ window, peaks U and V differ by ∼1.8 eV, close to the spin−orbit splitting between $Cl_{3/2}$ and $Cl_{1/2}$ in CH_2ICl, and these peaks are assigned as Cl($2p_{3/2}$) → σ^*(C−Cl) and Cl($2p_{1/2}$) → σ^*(C−Cl), respectively. They are blue-shifted by ∼0.6 eV from peaks E and F. Another two shoulder features labeled W and X, also split by ∼1.8 eV, resemble the Rydberg states G and I in Figure 1, also blue-shifted. The C−Cl bond distance is shortened when the radical is produced,[34−39] indicating a stronger C−Cl bond in the radical and thus greater absorption energies to σ^*(C−Cl). While the iodine atom departs the dihalomethane molecule, the electron density withdrawn by the iodine atom is given back to the carbon atom and possibly also the chlorine atom, which could have resulted in a lower halogen core binding energy and red-shifted Cl($2p_{1/2,\ 3/2}$) → σ^*(C−Cl) resonances. The blue shift shows that the shift in the valence bonding orbital is greater than the core shift in the chlorine atom, in contrast to the situation at the carbon atom.

Transitions from multiple core shells are captured simultaneously in this experiment, in this case to a common antibonding orbital in the radical, as summarized by the energies in Table 3 and the scheme drawn in Figure 5. When

Table 3. Summary of Spectral Features Associated with CH_2Cl[a]

peak	exptl. energy (eV)	assignment
J	282.8 ± 0.1	C(1s) → C(2p)
S	287.4 ± 0.2	C(1s) → σ^*(C−Cl)
T	289.8 ± 0.3	C(1s) → σ^*(C−H)
U	201.2 ± 0.3	Cl($2p_{3/2}$) → σ^*(C−Cl)
V	203.0 ± 0.3	Cl($2p_{1/2}$) → σ^*(C−Cl)

[a]Peak positions are reported as the averaged Gaussian fitting results of trials on different days. The errors are one standard deviation of those trials convoluted with Gaussian fitting errors.

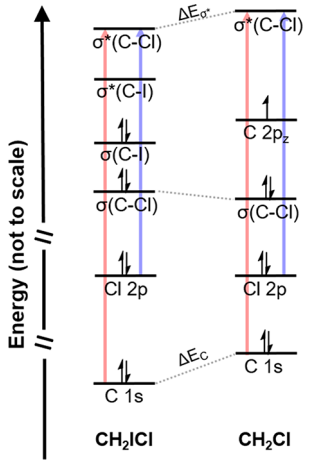

Figure 5. Schematic diagram of the molecular orbitals involved in the parent molecule CH_2ICl and the product CH_2Cl radical where C(1s) → σ^*(C−Cl) is red-shifted and Cl(2p) → σ^*(C−Cl) blue-shifted going from CH_2ICl to CH_2Cl.

CH_2ICl photodissociates into CH_2Cl at 266 nm, the C−Cl bond is strengthened, associated with a shift (ΔE_{σ^*}) in the valence σ^*(C−Cl) orbital, reflected in the blue shift of the Cl($2p_{1/2,\ 3/2}$) → σ^*(C−Cl) transitions. Meanwhile, the red shift in the C(1s) → σ^*(C−Cl) transition signifies that the shift in the carbon 1s core energy (ΔE_C) due to disappearance of the electron-withdrawing effect from iodine is larger than the shift in σ^*(C−Cl), that is, $\Delta E_C - \Delta E_{\sigma^*} = \sim 0.8$ eV.

DOI: 10.1021/jacs.8b08303
J. Am. Chem. Soc. 2018, 140, 13360−13366

CONCLUSION

Ultrafast core-level transient absorption spectroscopy combined with a selective bond breaking UV source has allowed the capture of transient radical species. As an example, photodissociation of CH_2ICl into CH_2Cl radical at 266 nm has been studied at both the carbon K edges and chlorine $L_{2,3}$ edge. The CH_2Cl radical thus produced is characterized by a prominent new carbon 1s → 2p feature at 282.8 ± 0.1 eV. The difference in the SOMO between the CH_3 and the CH_2Cl radical is explained by the electron-withdrawing effect of chlorine. Removal of an iodine atom also changes the oxidation state of the carbon atom, well reflected in the absorption spectra of CH_2ICl and CH_2Cl at the carbon K edge, a manifestation of valence electrons screening core electrons. In contrast, it imposes only a secondary impact on the chlorine core where the changes in the valence antibonding orbital and shorter C−Cl bond distance govern the core-to-valence transitions in chlorine. This paves the way for further studies on radicals where various types of radicals can be produced by selective bond breaking and substitution or stabilization effects on the SOMO and other valence orbitals can be quantified.

ASSOCIATED CONTENT

Supporting Information

The Supporting Information is available free of charge on the ACS Publications website at DOI: 10.1021/jacs.8b08303.

Experimental methods; spectral and temporal resolution determination; overview of CH_2ICl absorption spectra; kinetic fits of transient absorption data; transient absorption data with suppressed ion signals (PDF)

AUTHOR INFORMATION

Corresponding Author

*srl@berkeley.edu

ORCID

Zheyue Yang: 0000-0002-3446-0860
John F. Stanton: 0000-0003-2345-9781
Stephen R. Leone: 0000-0003-1819-1338

Present Addresses

#Paul Scherrer Institute, 5232 Villigen, Switzerland
⊥School of Chemistry, University of Bristol, Bristol BS8 1TH, United Kingdom

Notes

The authors declare no competing financial interest.

ACKNOWLEDGMENTS

Z.Y., A.B., M.E., T.X., and S.R.L. were funded by the U.S. Department of Energy, Office of Science, Office of Basic Energy Sciences under contract no. DE-AC02-05CH11231. K.S. was funded by a Peter Paul Ewald Fellowship from the Volkswagen Foundation. J.F.S. was supported by the U.S. Department of Energy, Office of Science, Office of Basic Energy Sciences under contract DE-FG02-07ER15884.

REFERENCES

(1) Enami, S.; Hoffmann, M. R.; Colussi, A. J. Halogen Radical Chemistry at Aqueous Interfaces. *J. Phys. Chem. A* **2016**, *120* (31), 6242−6248.

(2) Marshall, P.; Srinivas, G. N.; Schwartz, M. A computational study of the thermochemistry of bromine- and iodine-containing methanes and methyl radicals. *J. Phys. Chem. A* **2005**, *109* (28), 6371−6379.

(3) Olleta, A. C.; Lane, S. I. Ab initio studies of the gas-phase thermodynamic properties and bond dissociation energies for haloethanes and halomethyl radicals. *Phys. Chem. Chem. Phys.* **2001**, *3* (5), 811−818.

(4) Violi, A.; D'Anna, A.; D'Alessio, A. A modeling evaluation of the effect of chlorine on the formation of particulate matter in combustion. *Chemosphere* **2001**, *42* (5−7), 463−471.

(5) Hung, S. L.; Pfefferle, L. D. A Flow Tube Kinetics Study of Methyl-Chloride Oxidation. *Combust. Sci. Technol.* **1993**, *87* (1−6), 91−107.

(6) Molina, M. J.; Rowland, F. S. Stratospheric Sink for Chlorofluoromethanes - Chlorine Atomic-Catalysed Destruction of Ozone. *Nature* **1974**, *249* (5460), 810−812.

(7) Rattigan, O. V.; Shallcross, D. E.; Cox, R. A. UV absorption cross-sections and atmospheric photolysis rates of CF_3I, CH_3I, C_2H_5I and CH_2ICl. *J. Chem. Soc., Faraday Trans.* **1997**, *93* (16), 2839−2846.

(8) Attar, A. R.; Bhattacherjee, A.; Pemmaraju, C. D.; Schnorr, K.; Closser, K. D.; Prendergast, D.; Leone, S. R. Femtosecond x-ray spectroscopy of an electrocyclic ring-opening reaction. *Science* **2017**, *356* (6333), 54−58.

(9) Bhattacherjee, A.; Das Pennaraju, C.; Schnorr, K.; Attar, A. R.; Leone, S. R. Ultrafast Intersystem Crossing in Acetylacetone via Femtosecond X-ray Transient Absorption at the Carbon K-Edge. *J. Am. Chem. Soc.* **2017**, *139* (46), 16576−16583.

(10) Pertot, Y.; Schmidt, C.; Matthews, M.; Chauvet, A.; Huppert, M.; Svoboda, V.; von Conta, A.; Tehlar, A.; Baykusheva, D.; Wolf, J. P.; Worner, H. J. Time-resolved x-ray absorption spectroscopy with a water window high-harmonic source. *Science* **2017**, *355* (6322), 264−267.

(11) Senapati, D.; Kavita, K.; Das, P. K. Photodissociation dynamics of CH2ICl at 222, 236, 266, 280, and-304 nm. *J. Phys. Chem. A* **2002**, *106* (36), 8479−8482.

(12) Murillo-Sanchez, M. L.; Poullain, S. M.; Gonzalez-Vazquez, J.; Corrales, M. E.; Balerdi, G.; Banares, L. Femtosecond photodissociation dynamics of chloroiodomethane in the first absorption band. *Chem. Phys. Lett.* **2017**, *683*, 22−28.

(13) Murillo-Sánchez, M. L.; Marggi Poullain, S.; Bajo, J. J.; Corrales, M. E.; González-Vázquez, J.; Solá, I. R.; Bañares, L. Halogen-atom effect on the ultrafast photodissociation dynamics of the dihalomethanes CH2ICl and CH2BrI. *Phys. Chem. Chem. Phys.* **2018**, *20* (32), 20766−20778.

(14) King, G. C.; Tronc, M.; Read, F. H.; Bradford, R. C. Investigation of Structure near $L_{2,3}$ Edges of Argon, $M_{4,5}$ Edges of Krypton and $N_{4,5}$ Edges of Xenon, Using Electron-Impact with High-Resolution. *J. Phys. B: At. Mol. Phys.* **1977**, *10* (12), 2479−2495.

(15) Hedin, L.; Eland, J. H. D.; Karlsson, L.; Feifel, R. An x-ray absorption and a normal Auger study of the fine structure in the S $2p^{-1}$ region of the CS_2 molecule. *J. Phys. B: At., Mol. Opt. Phys.* **2009**, *42* (8), 085102.

(16) Wight, G. R.; Brion, C. E. K- and $L_{II,III}$-Shell Excitations in CS_2 and COS by 2.5 Kev Electron-Impact. *J. Electron Spectrosc. Relat. Phenom.* **1974**, *4* (4), 335−345.

(17) Hitchcock, A. P.; Brion, C. E. Assignment of the Carbon K-Shell Spectra of the Methyl Halides. *J. Electron Spectrosc. Relat. Phenom.* **1979**, *17* (3), 139−147.

(18) Saeh, J. C.; Stanton, J. F. Application of an equation-of-motion coupled cluster method including higher-order corrections to potential energy surfaces of radicals. *J. Chem. Phys.* **1999**, *111* (18), 8275−8285.

(19) Stanton, J. F.; Gauss, J. A simple correction to final state energies of doublet radicals described by equation-of-motion coupled cluster theory in the singles and doubles approximation. *Theor Chim Acta* **1996**, *93* (5), 303−313.

(20) Dyall, K. G. Interfacing relativistic and nonrelativistic methods 0.1. Normalized elimination of the small component in the modified Dirac equation. *J. Chem. Phys.* **1997**, *106* (23), 9618−9626.

DOI: 10.1021/jacs.8b08303
J. Am. Chem. Soc. 2018, 140, 13360−13366

(21) Liu, W. J.; Peng, D. L. Exact two-component Hamiltonians revisited. *J. Chem. Phys.* **2009**, *131* (3), 031104.
(22) Cheng, L.; Gauss, J. Analytic energy gradients for the spin-free exact two-component theory using an exact block diagonalization for the one-electron Dirac Hamiltonian. *J. Chem. Phys.* **2011**, *135* (8), 084114.
(23) Roos, B. O.; Lindh, R.; Malmqvist, P. A.; Veryazov, V.; Widmark, P. O. New relativistic ANO basis sets for transition metal atoms. *J. Phys. Chem. A* **2005**, *109* (29), 6575−6579.
(24) Stanton, J. F.; Gauss, J.; Cheng, L.; Harding, M. E.; Matthews, D. A.; Szalay, P. G., *CFOUR, coupled-cluster techniques for computational chemistry*, www.cfour.de (accessed August 1, 2018).
(25) Musial, M.; Kucharski, S. A.; Bartlett, R. J. Equation-of-motion coupled cluster method with full inclusion of the connected triple excitations for ionized states: IP-EOM-CCSDT. *J. Chem. Phys.* **2003**, *118* (3), 1128−1136.
(26) Alagia, M.; Lavollee, M.; Richter, R.; Ekstrom, U.; Carravetta, V.; Stranges, D.; Brunetti, B.; Stranges, S. Probing the potential energy surface by high-resolution x-ray absorption spectroscopy: The umbrella motion of the core-excited CH_3 free radical. *Phys. Rev. A: At., Mol., Opt. Phys.* **2007**, *76* (2), 022509.
(27) Hitchcock, A. P.; Brion, C. E. Inner-Shell Excitation and Exafs-Type Phenomena in Chloromethanes. *J. Electron Spectrosc. Relat. Phenom.* **1978**, *14* (6), 417−441.
(28) O'Sullivan, G. Chlorine L-Edge Absorption in CCl_4 and CCl_2F_2. *J. Phys. B: At. Mol. Phys.* **1982**, *15* (15), 2385−2390.
(29) Hitchcock, A. P.; Brion, C. E. Inner Shell Excitation of CH_3F, CH_3Cl, CH_3Br and CH_3I by 2.5 Kev Electron-Impact. *J. Electron Spectrosc. Relat. Phenom.* **1978**, *13* (3), 193−218.
(30) Degroot, F. M. F. Differences between L_3 and L_2 X-Ray-Absorption Spectra. *Phys. B* **1995**, *208* (1−4), 15−18.
(31) Attar, A. R.; Piticco, L.; Leone, S. R. Core-to-valence spectroscopic detection of the CH_2Br radical and element-specific femtosecond photodissociation dynamics of CH_2IBr. *J. Chem. Phys.* **2014**, *141* (16), 164308.
(32) Lago, A. F.; Kercher, J. P.; Bodi, A.; Sztaray, B.; Miller, B.; Wurzelmann, D.; Baer, T. Dissociative photoionization and thermochemistry of dihalomethane compounds studied by threshold photoelectron photoion coincidence spectroscopy. *J. Phys. Chem. A* **2005**, *109* (9), 1802−1809.
(33) Loh, Z. H.; Leone, S. R. Ultrafast strong-field dissociative ionization dynamics of CH_2Br_2 probed by femtosecond soft x-ray transient absorption spectroscopy. *J. Chem. Phys.* **2008**, *128* (20), 204302.
(34) Li, Z. J.; Francisco, J. S. High level ab initio molecular orbital study of the structures and vibrational spectra of CH_2Br and CH_2Br^+. *J. Chem. Phys.* **1999**, *110* (2), 817−822.
(35) Bailleux, S.; Duflot, D.; Taniguchi, K.; Sakai, S.; Ozeki, H.; Okabayashi, T.; Bailey, W. C. Fourier Transform Microwave and Millimeter-Wave Spectroscopy of Bromoiodomethane, CH_2BrI. *J. Phys. Chem. A* **2014**, *118* (50), 11744−11750.
(36) Li, Y. M.; Francisco, J. S. CASSCF and MRCl studies of the electronic excited states of CH_2Cl and CH_2Br. *J. Chem. Phys.* **2001**, *114* (7), 2879−2882.
(37) Levchenko, S. V.; Krylov, A. I. Electronic structure of halogen-substituted methyl radicals: Equilibrium geometries and vibrational spectra of CH_2Cl and CH_2F. *J. Phys. Chem. A* **2002**, *106* (20), 5169−5176.
(38) Kim, H.; Park, Y. C.; Lee, Y. S. Spin-orbit Effects on the Structure of Haloiodomethane Cations CH_2XI^+ (X = F, Cl, Br, and I). *Bull. Korean Chem. Soc.* **2014**, *35* (3), 775−782.
(39) Ohkoshi, I.; Niide, Y.; Takano, M. Microwave-Spectrum and Quadrupole Coupling-Constant Tensor of Chloroiodomethane. *J. Mol. Spectrosc.* **1987**, *124* (1), 118−129.

DOI: 10.1021/jacs.8b08303
J. Am. Chem. Soc. 2018, 140, 13360−13366